A machine learning approach to evaluate the influence of higher-order generalized variables on shell free vibrations

Journal of Sound and Vibration 575 (2024) 118255

Contents lists available at ScienceDirect

Journal of Sound and Vibration

journal homepage: www.elsevier.com/locate/jsvi

A machine learning approach to evaluate the influence of higher-order generalized variables on shell free vibrations

M. Petrolo [*,1], P. Iannotti[1], M. Trombini[1], A. Pagani[1], E. Carrera[1]

MUL² Lab, Department of Mechanical and Aerospace Engineering, Politecnico di Torino, Corso Duca degli Abruzzi 24, 10129 Torino, Italy

ARTICLE INFO

Keywords:
CUF
Structural theories
Shells
Composites
Neural networks
FEM

ABSTRACT

This work focuses on deriving guidelines for choosing structural theories for composite shells using Convolutional Neural Networks (CNN). The Axiomatic/Asymptotic Method (AAM) is used to evaluate higher-order structural theories' accuracy and computational efficiency based on polynomial expansions. AAM exploits the Carrera Unified Formulation to derive the finite element matrices and obtain natural frequencies. The outcomes of AAM concerning the accuracy and computational cost are used to train CNN for various composite shell configurations. The trained network can then be used as a substitute for finite element models to estimate the accuracy of a given structural theory. The results are provided via Best Theory Diagrams (BTD), in which the set of generalized displacement variables to retain the best accuracy can be read for a given amount of nodal degrees of freedom. Verification is carried out using results from FEM. The results proved the computational efficiency of CNN and highlighted the influence of the shell thickness for the proper choice of the structural theory. Third-order terms and transverse stretching are often necessary to obtain acceptable accuracy.

1. Introduction

Modeling composite structures requires a trade-off between accuracy and computational overhead. Focusing on 2D theories of composite plates and shells, numerical models must deal with several mechanical behaviors, such as transverse anisotropy and shear deformability. One approach is the use of an increasing number of generalized unknown variables, i.e., the nodal degrees of freedoms, through higher-order polynomial thickness expansions [1–4] or the inclusion of non-polynomial terms [5–8]. The structural theories originated from this approach, often referred to as higher-order theories (HOT), approximate the laminate as an Equivalent Single Layer (ESL), meaning that the amount of adopted variables is independent of the number of layers. This specific family of theories is a valuable tool due to their flexibility and practically unlimited variety, given that different expansions can be used for each displacement component. Their accuracy is strictly problem dependent, and a systematic approach to selecting the suitable model for the considered application is desirable. The Axiomatic/Asymptotic Method (AAM) [9–11] can be directly applied to higher-order theories to identify the best models for different levels of numerical complexity. The first step of this process is the axiomatic choice of a maximum order of the polynomial expansions, with the complete one being usually assumed as the reference model. Terms are then suppressed, and for each expansion, a level of accuracy can be evaluated with respect to the reference solution. A fundamental aspect of this approach is the definition of the accuracy parameter. As shown in other works [12–14], depending on how the precision error is evaluated, different theories can emerge as the optimal ones for the same structural problem, further improving

* Corresponding author.
E-mail address: marco.petrolo@polito.it (M. Petrolo).
[1] Contribute equally to this paper.

https://doi.org/10.1016/j.jsv.2024.118255
Received 8 June 2023; Received in revised form 28 December 2023; Accepted 6 January 2024
Available online 11 January 2024

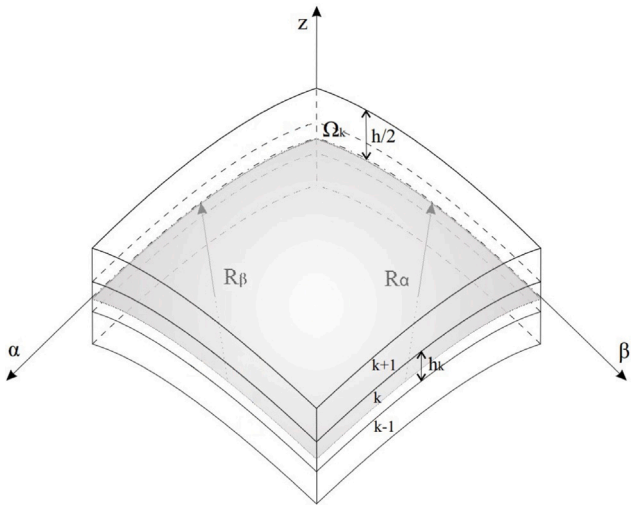

Fig. 1. Reference geometry for shell models.

the capabilities of higher-order ESL models. The AAM requires the comparison of all possible combinations of terms up to the fixed order of expansion, and this can make its implementation computationally expensive in the case of more complex structures, mainly due to the computational efforts needed to evaluate such a large number of solutions. A possible way to derive information about the best theory to adopt for a specific problem in a much more convenient way can be found in the use of Machine Learning (ML) techniques, specifically Neural Networks (NN) [15,16]. The use and capabilities of these mathematical tools have been growing in the last years in many different fields, also including structural mechanics [17–25]. This paper uses a specific family of NN, Convolutional Neural Networks (CNN) [26–28]. The aim is to exploit the superior capabilities of CNN to include multiple problem features in the training process and create a surrogate model able to substitute FEM analysis to compute natural frequencies. Such a result is desirable to lower the computational cost of the AAM approach and generalize the results obtained. The former goal may be achieved by using only a fraction of FEM results to train the network; the latter by incorporating multiple features, e.g., boundary conditions and thickness, and obtaining multiple outputs, e.g., natural frequencies. Stemming from the methodology and results described in [29–31], the approach is based on the Carrera Unified Formulation (CUF) [32], an efficient and generalized way to derive the governing equations for virtually any structural theory and related finite element formulation. Here, for the first time, CNN is applied to obtain the Best Theory Diagrams (BTD) for various composite plate and shell configurations utilizing the accuracy in estimating different natural frequencies of the structure. This selection can be made at a fraction of the cost required by the full implementation of the AAM by simply reducing the necessary results to perform such an evaluation. The paper has the following structure: Section 2 briefly goes over the CUF and the considered structural models, Section 3 presents the AAM and the concepts of the Best Theory Diagram, Section 4 describes the architecture and the use of the CNN, while results and conclusions are presented in Sections 5 and 6, respectively.

2. Carrera Unified Formulation and finite elements

The structural theories analyzed in this paper were obtained using the Carrera Unified Formulation. The starting point for describing the adopted modeling approach based on the CUF is the definition of the reference system. The one used for 2D multi-layered shell models is presented in Fig. 1. The reference frame is curvilinear, with α and β coinciding with the principal curvature lines and z along the thickness. Doubly curved shells were considered, with the curvature radii R_α and R_β. Ω_k refers to the mid-surface of the kth layer, with h_k being its thickness.

The analyzed models are built using expansion functions of the displacement field. In the framework of the CUF, it is possible to build refined 2D models with an advanced description of the through-the-thickness mechanical behavior by introducing so-called expansion functions F_τ. The displacement field can then be expressed as:

$$\mathbf{u}(\alpha,\beta,z) = (u_\alpha, u_\beta, u_z) = F_\tau(z)\mathbf{u}_\tau(\alpha,\beta) \qquad \tau = 0,\dots,N \tag{1}$$

with N being the number of terms of the expansion and u_τ the set of generalized displacement unknowns. The Einstein notation is used on τ and similarly is done throughout the entirety of this section. For reference, a fourth-order expansion based on Taylor polynomials used on all three displacement components is:

$$\begin{aligned} u_\alpha &= u_{\alpha_1} + z\,u_{\alpha_2} + z^2\,u_{\alpha_3} + z^3\,u_{\alpha_4} + z^4\,u_{\alpha_5} \\ u_\beta &= u_{\beta_1} + z\,u_{\beta_2} + z^2\,u_{\beta_3} + z^3\,u_{\beta_4} + z^4\,u_{\beta_5} \\ u_z &= u_{z_1} + z\,u_{z_2} + z^2\,u_{z_3} + z^3\,u_{z_4} + z^4\,u_{z_5} \end{aligned} \tag{2}$$

The FE formulation of the displacement field uses the shape functions N_i for the interpolation on the nodes of the elements and accounts for the kth layer,

$$\mathbf{u}^k(\alpha,\beta,z) = F_\tau^k(z) N_i(\alpha,\beta)\mathbf{u}_{\tau i}^k \qquad \tau = 0,\dots,N \quad i = 1,\dots,N_n \tag{3}$$

where N_n is the number of nodes of the element and $u_{\tau i}^k$ are the nodal generalized displacement variables. The variation of the displacement field can be written as:

$$\delta\mathbf{u}^k(\alpha,\beta,z) = F_s^k(z) N_j(\alpha,\beta)\delta\mathbf{u}_{sj}^k \qquad s = 0,\dots,N \quad j = 1,\dots,N_n \tag{4}$$

The in-plane, $\boldsymbol{\epsilon}_p^k$, and out-plane, $\boldsymbol{\epsilon}_n^k$, strain components can be obtained through the following geometric relations:

$$\boldsymbol{\epsilon}_p^k = \left\{ \epsilon_{\alpha\alpha}^k, \epsilon_{\beta\beta}^k, \epsilon_{\alpha\beta}^k \right\}^T = (\mathbf{D}_p^k + \mathbf{A}_p^k)\mathbf{u}^k \tag{5}$$

$$\boldsymbol{\epsilon}_n^k = \left\{ \epsilon_{\alpha z}^k, \epsilon_{\beta z}^k, \epsilon_{zz}^k \right\}^T = (\mathbf{D}_{n\Omega}^k + \mathbf{D}_{nz}^k - \mathbf{A}_n^k)\mathbf{u}^k \tag{6}$$

The matrices $\mathbf{D}_p^k$, $\mathbf{D}_{n\Omega}^k$, $\mathbf{D}_{nz}^k$, $\mathbf{A}_p^k$, and $\mathbf{A}_n^k$ are:

$$\mathbf{D}_p^k = \begin{bmatrix} \frac{\partial_\alpha}{H_\alpha^k} & 0 & 0 \\ 0 & \frac{\partial_\beta}{H_\beta^k} & 0 \\ \frac{\partial_\beta}{H_\beta^k} & \frac{\partial_\alpha}{H_\alpha^k} & 0 \end{bmatrix} \quad \mathbf{D}_{n\Omega}^k = \begin{bmatrix} 0 & 0 & \frac{\partial_\alpha}{H_\alpha^k} \\ 0 & 0 & \frac{\partial_\beta}{H_\beta^k} \\ 0 & 0 & 0 \end{bmatrix} \quad \mathbf{D}_{nz}^k = \begin{bmatrix} \partial_z & 0 & 0 \\ 0 & \partial_z & 0 \\ 0 & 0 & \partial_z \end{bmatrix} \tag{7}$$

$$\mathbf{A}_p^k = \begin{bmatrix} 0 & 0 & \frac{1}{H_\alpha^k R_\alpha^k} \\ 0 & 0 & \frac{1}{H_\beta^k R_\beta^k} \\ 0 & 0 & 0 \end{bmatrix} \quad \mathbf{A}_n^k = \begin{bmatrix} \frac{1}{H_\alpha^k R_\alpha^k} & 0 & 0 \\ 0 & \frac{1}{H_\beta^k R_\beta^k} & 0 \\ 0 & 0 & 0 \end{bmatrix} \tag{8}$$

H_α^k and H_β^k are defined as:

$$H_\alpha^k = A^k(1 + z_k/R_\alpha^k) \tag{9}$$

$$H_\beta^k = B^k(1 + z_k/R_\beta^k) \tag{10}$$

A^k and B^k are the coefficients of the first fundamental form of Ω_k, and z_k is the thickness coordinate through the kth layer. For shells with constant radii of curvature, A^k=B^k=1. A more extensive description of these geometrical parameters can be found in [33].

In this paper, shell finite elements with nine nodes were used and obtained through Lagrange shape functions to interpolate the displacements. Shape functions are defined on a local reference system of the nine-node element - $-1 \le \xi, \eta \le 1$ - as shown in Fig. 2, and their explicit form can be found in [34]. According to the FE formulation, the geometric relations become:

$$\boldsymbol{\epsilon}_p^k = F_\tau(\mathbf{D}_p^k + \mathbf{A}_p^k)(N_i\mathbf{I})\mathbf{u}_{\tau i}^k \tag{11}$$

$$\boldsymbol{\epsilon}_n^k = F_\tau(\mathbf{D}_{n\Omega}^k - \mathbf{A}_n^k)(N_i\mathbf{I})\mathbf{u}_{\tau i}^k + F_{\tau,z}(N_i\mathbf{I})\mathbf{u}_{\tau i}^k \tag{12}$$

where $\mathbf{I}$ is identity matrix. This paper adopted the Mixed Interpolation of Tensorial Components (MITC) approach [35,36]. According to this formulation, the strain components are obtained through specific interpolation strategies. First, three sets of interpolation points – referred to as "tying points" – are defined in the element local coordinate system. Each set of points is used for the interpolation of different strain components, as explicitly indicated in Fig. 3, and this is done through their respective interpolation functions. The interpolation functions can be conveniently grouped as follows:

$$\begin{aligned} \mathbf{N}_{m1} &= [N_{A1}, N_{B1}, N_{C1}, N_{D1}, N_{E1}, N_{F1}] \\ \mathbf{N}_{m2} &= [N_{A2}, N_{B2}, N_{C2}, N_{D2}, N_{E2}, N_{F2}] \\ \mathbf{N}_{m3} &= [N_P, N_Q, N_R, N_S] \end{aligned} \tag{13}$$

For further details on the mathematical formulation of MITC, the reader can refer to [34]. The strain components are interpolated as follows:

$$\boldsymbol{\epsilon}_p^k = \begin{bmatrix} \mathbf{N}_{m1} & 0 & 0 \\ 0 & \mathbf{N}_{m2} & 0 \\ 0 & 0 & \mathbf{N}_{m3} \end{bmatrix} \begin{bmatrix} \boldsymbol{\epsilon}_{\alpha\alpha_{m1}} \\ \boldsymbol{\epsilon}_{\beta\beta_{m2}} \\ \boldsymbol{\epsilon}_{\alpha\beta_{m3}} \end{bmatrix} \tag{14}$$

$$\boldsymbol{\epsilon}_n^k = \begin{bmatrix} \mathbf{N}_{m1} & 0 & 0 \\ 0 & \mathbf{N}_{m2} & 0 \\ 0 & 0 & 1 \end{bmatrix} \begin{bmatrix} \boldsymbol{\epsilon}_{\alpha z_{m1}} \\ \boldsymbol{\epsilon}_{\beta z_{m2}} \\ \boldsymbol{\epsilon}_{zz} \end{bmatrix} \tag{15}$$

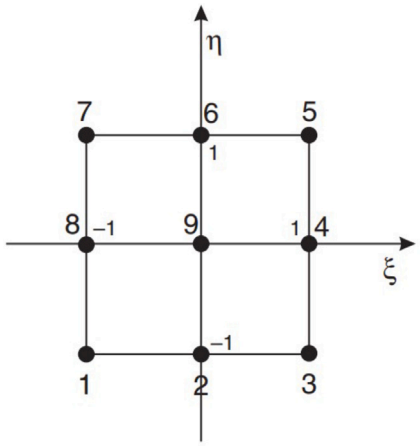

Fig. 2. Nine-node finite element, Q9.

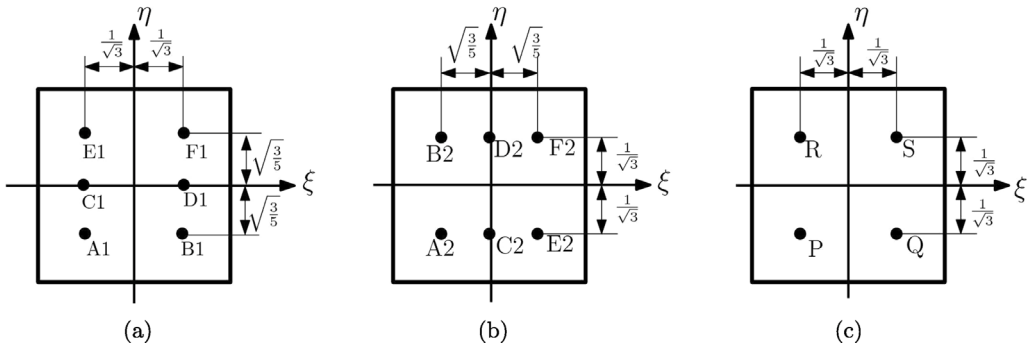

Fig. 3. MITC9 tying points for different strain components - (a) Interpolation of $\epsilon_{\alpha\alpha}$ and $\epsilon_{\alpha z}$, (b) Interpolation of $\epsilon_{\beta\beta}$ and $\epsilon_{\beta z}$, (c) Interpolation of $\epsilon_{\alpha\beta}$.

Subscripts m_1, m_2, and m_3 refer to quantities evaluated in the tying points of the respective group. The strain components at the tying points, e.g., $\boldsymbol{\epsilon}_{\alpha\alpha_{m1}}$, must be evaluated directly from the displacements using Eqs. (5) and (6). As an example, $\epsilon_{\alpha\alpha}$ becomes

$$\epsilon_{\alpha\alpha} = N_{A1}\epsilon_{\alpha\alpha_{A1}} + N_{B1}\epsilon_{\alpha\alpha_{B1}} + N_{C1}\epsilon_{\alpha\alpha_{C1}} + N_{D1}\epsilon_{\alpha\alpha_{D1}} + N_{E1}\epsilon_{\alpha\alpha_{E1}} + N_{F1}\epsilon_{\alpha\alpha_{F1}} \tag{16}$$

where

$$\epsilon_{\alpha\alpha} = N^{(A1)}_{i,\alpha} F_\tau u_{\alpha\tau_i} + \frac{1}{H_\alpha R_\alpha} N^{(A1)}_i F_\tau u_{z\tau_i}. \tag{17}$$

The superscript, A_1, indicates where the shape function and its derivative - $_{,\alpha}$ - are evaluated.

Hooke's law is considered for the definition of the constitutive equations. For an orthotropic material, isolating in-plane and normal stress components, it holds:

$$\boldsymbol{\sigma}^k_p = \boldsymbol{C}^k_{pp}\boldsymbol{\epsilon}^k_p + \boldsymbol{C}^k_{pn}\boldsymbol{\epsilon}^k_n \tag{18}$$

$$\boldsymbol{\sigma}^k_n = \mathbf{C}^k_{np}\boldsymbol{\epsilon}^k_p + \mathbf{C}^k_{nn}\boldsymbol{\epsilon}^k_n \tag{19}$$

The material coefficient matrices are defined as follows:

$$\begin{aligned}
\mathbf{C}^k_{pp} &= \begin{bmatrix} C^k_{11} & C^k_{12} & C^k_{16} \\ C^k_{12} & C^k_{22} & C^k_{26} \\ C^k_{16} & C^k_{26} & C^k_{66} \end{bmatrix} \quad \mathbf{C}^k_{pn} = \begin{bmatrix} 0 & 0 & C^k_{13} \\ 0 & 0 & C^k_{23} \\ 0 & 0 & C^k_{36} \end{bmatrix} \\
\mathbf{C}^k_{np} &= \begin{bmatrix} 0 & 0 & 0 \\ 0 & 0 & 0 \\ C^k_{13} & C^k_{23} & C^k_{36} \end{bmatrix} \quad \mathbf{C}^k_{nn} = \begin{bmatrix} C^k_{55} & C^k_{45} & 0 \\ C^k_{45} & C^k_{44} & 0 \\ 0 & 0 & C^k_{33} \end{bmatrix}
\end{aligned} \tag{20}$$

The coefficients C_{ij} are functions of Young's moduli E_1, E_2, E_3, Poisson's ratios ν_{12}, ν_{13}, ν_{23}, and shear moduli G_{12}, G_{13}, G_{23}. For each layer, these equations are first considered in the material coordinates – 1, 2, 3 – then rotated to the global curvilinear coordinates system — α, β, z. The explicit form of each C_{ij} coefficient is not reported for brevity, but they can be found in [37,38]. Constitutive and geometrical relations are substituted in the Principle of Virtual Displacements (PVD) to obtain the governing differential equations,

$$\delta L_{\text{int}} = \delta L_{\text{ext}} - \delta L_{\text{ine}} \tag{21}$$

L_{int} is the work done by internal forces, L_{ext} is the work done by the external forces, and L_{ine} is the inertial work. For a multilayered shell and in the case of free-vibrations, Eq. (21) becomes:

$$\int_{\Omega_k}\int_{A_k} \delta\boldsymbol{\epsilon}^{k^T}\boldsymbol{\sigma}^k H^k_\alpha H^k_\beta \mathrm{d}\Omega_k \mathrm{d}z + \int_{\Omega_k}\int_{A_k} \rho^k \delta\boldsymbol{u}^{k^T}\ddot{\boldsymbol{u}}^k H^k_\alpha H^k_\beta \mathrm{d}\Omega_k \mathrm{d}z = 0 \tag{22}$$

ρ^k is the mass density of the kth layer, Ω_k and A_k are the integration domains over α, β, and z, T indicates the transpose of a vector, and the double dots the acceleration. By substituting strains and stresses in Eq. (22) and describing the displacement field through the FE formulation defined in Eq. (3), the variations of the internal and inertial works can be rewritten as:

$$\delta L^k_{\text{int}} = \delta \mathbf{u}^{k^T}_{sj} \mathbf{k}^{k\tau sij} \mathbf{u}^k_{\tau i} \tag{23}$$

$$\delta L^k_{\text{ine}} = \delta \mathbf{u}^{k^T}_{sj} \mathbf{m}^{k\tau sij} \ddot{\mathbf{u}}^k_{\tau i} \tag{24}$$

where $\mathbf{k}^{k\tau sij}$ and $\mathbf{m}^{k\tau sij}$ are the stiffness and mass matrices in the form of fundamental nuclei (FN). FN are 3×3 arrays working as basic assembly units and are formally independent of the order of the structural theory,

$$\mathbf{k}^{k\tau sij} = \begin{bmatrix} k^{k\tau sij}_{\alpha\alpha} & k^{k\tau sij}_{\alpha\beta} & k^{k\tau sij}_{\alpha z} \\ k^{k\tau sij}_{\beta\alpha} & k^{k\tau sij}_{\beta\beta} & k^{k\tau sij}_{\beta z} \\ k^{k\tau sij}_{z\alpha} & k^{k\tau sij}_{z\beta} & k^{k\tau sij}_{zz} \end{bmatrix} \tag{25}$$

The explicit expressions for each term of the mass and stiffness fundamental nuclei can be found in [34,39]. The FE matrices can be obtained by cycling over the four indexes (τ, s, i, j). Once the matrices for each layer are obtained, they can be assembled depending on the modeling approach considered. Only Equivalent-Single Layer (ESL) models were analyzed in this paper, meaning that a single set of unknown variables is used across the entire thickness, independently of the number of layers in the structure. The governing equation for the free-vibration problem can finally be rewritten as:

$$\mathbf{m}^{k\tau sij}\ddot{\mathbf{u}}_{\tau i} + \mathbf{k}^{k\tau sij}\mathbf{u}_{\tau i} = 0 \tag{26}$$

The assembly over all nodes and elements and the introduction of the harmonic solution leads to the well-known eigenvalue problem,

$$(-\omega_n^2 \boldsymbol{M} + \boldsymbol{K})\boldsymbol{U}_n = 0 \tag{27}$$

with $\mathbf{U}_n$ being the nth eigenvector and ω_n the nth angular frequency.

3. Axiomatic/Asymptotic method

The Axiomatic/Asymptotic Method is an approach to analyze the influence of generalized variables on the solution and select the most convenient structural theory for best accuracy and lowest computational cost [12–14,40]. This paper uses AAM with structural theories based on polynomial expansions of unknown variables. A fourth-order expansion was chosen as the highest order as it delivers high accuracy for the problem under consideration. In this scenario, 2^{15} possible structural theories can be derived by selecting various combinations of expansion terms. It is essential to mention that this tally includes the arrangement where all terms are deactivated, but this configuration is excluded from consideration as irrelevant. Among the remaining 2^{15}-1 theories, only those featuring the activation of three constant terms were considered since these are crucial for significant results. Consequently, the total number of possible combinations is 2^{12}. The accuracy of a theory can be evaluated as a percentage error over a quantity of interest, such as displacements or natural frequencies. However, the large amount of required FEM analyses may be a limiting factor, especially for complex structures. This work explores a possible solution to this issue by using Convolutional Neural Networks, drastically reducing the number of FEM results required to perform the selection procedure. The result of the AAM can be conveniently represented using the Best Theory Diagram, shown in Fig. 4. The BTD provides several pieces of information; namely, for a given number of DOF, it indicates the combination of generalized variables providing the minimum error; furthermore, it reports the lowest error obtainable for a given number of DOF. The BTD may be used to evaluate the accuracy of any theory; e.g., if five DOF are considered, the BTD may be used to assess the performance of FSDT. The control parameter used in this paper is the error over a single natural frequency,

$$\%E_{f_i} = 100 \times \frac{|f_i - f_i^{E4}|}{f_i^{E4}} \tag{28}$$

where f_i^{E4} is the ith frequency evaluated using a full fourth-order Taylor expansion. In previous works [40], the error measure was a mean value among those from the first ten frequencies, and the best models were built to obtain a given mean accuracy over the first

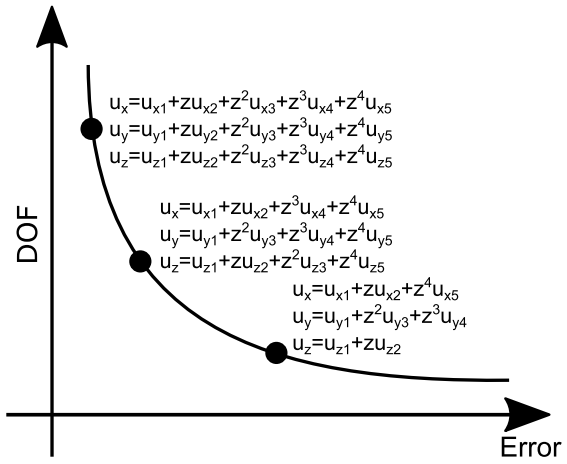

Fig. 4. Best Theory Diagram.

Table 1
Example of best theory representation.

DOF	$u_{\alpha 1}$	$u_{\beta 1}$	u_{z1}	$u_{\alpha 2}$	$u_{\beta 2}$	u_{z2}	$u_{\alpha 3}$	$u_{\beta 3}$	u_{z3}	$u_{\alpha 4}$	$u_{\beta 4}$	u_{z4}	$u_{\alpha 5}$	$u_{\beta 5}$	u_{z5}
8	▲	▲	▲	△	▲	△	▲	△	△	▲	▲	△	▲	△	△

ten frequencies. The present work evaluates how a given theory's accuracy can change depending on the modes. Such information may be helpful in various scenarios, e.g., when commercial codes are used in which the structural theory cannot be modified, and the user must be aware that, depending on the mode number, the accuracy can change. For every structural configuration considered, the resulting best theory for a given number of active DOF can be conveniently represented in tabular form using black and white triangles to indicate active and inactive terms, respectively, see Table 1. The model described in Table 1 has the following displacement field:

$$\begin{aligned} u_\alpha &= u_{\alpha_1} + z^2\, u_{\alpha_3} + z^3\, u_{\alpha_4} + z^4\, u_{\alpha_5} \\ u_\beta &= u_{\beta_1} + z\, u_{\beta_2} + z^3\, u_{\beta_4} \\ u_z &= u_{z_1} \end{aligned} \tag{29}$$

4. Convolutional Neural Network

The computational cost and time required by the AAM can be prohibitive, especially when dealing with larger structures. By taking advantage of the generalization capabilities of ML techniques, it is possible to reproduce the output of an Axiomatic/Asymptotic procedure with a drastic reduction in the number of required numerical results. In this work, the focus is on Convolutional Neural Networks (CNN) to identify the most influential expansion terms affecting the accuracy of solutions obtained from free-vibration analyses of composite shells. Specifically, a CNN is employed to compute the error in estimating the first ten natural frequencies using a given set of active generalized displacement variables. The errors were then used to obtain the BTD for different structural configurations. The trained CNN can, then, be used to evaluate the accuracy of a given structural theory, e.g., it may accept as an input the displacement field of FSDT and provide the error in computing the first ten natural frequencies. The creation, training, and testing of the CNN were performed using Python and the well-known libraries of Tensorflow and Keras. The network was designed to manage both multi-dimensional inputs and outputs. The input representation of each model was obtained by encoding the sequence of active generalized displacement variables of a specific structural theory into a series of 0 and 1, corresponding to a deactivated and active expansion term, respectively, e.g.,

$$\begin{aligned} u_\alpha &= u_{\alpha_1} + z\, u_{\alpha_2} + z^4\, u_{\alpha_5} \\ u_\beta &= u_{\beta_1} + z\, u_{\beta_2} + z^3\, u_{\beta_4} \quad \Rightarrow \quad [1\,1\,1\,0\,0\,1\,0\,1\,0\,1\,0\,0] \\ u_z &= u_{z_1} + z\, u_{z_2} + z^2\, u_{z_3} \end{aligned} \tag{30}$$

Constant terms were not included in the encoded sequence, as they were always set as active. The sequence was then re-shaped into a 3×4 matrix, constituting the actual input provided to the network. The complete architecture of the CNN is described in Table 2, and it resulted from numerous tests aimed at selecting the best-performing one for this specific application while also trying to keep the number of parameters relatively low. It presents a first block of three convolutional layers with 128 3×3 filters. All of them used a Rectified Linear Unit (ReLU) activation function. A uniform stride of 1 was used to perform the convolution, and padding was added to preserve the original size of the input through these layers, improving the network's capabilities. The output of the

Table 2
Parameters and architecture of the adopted CNN.

Layer	Filters (Size)/Nodes	Activation function
Convolutional	128 (3 × 3)	ReLU
Convolutional	128 (3 × 3)	ReLU
Convolutional	128 (3 × 3)	ReLU
Flatten	–	–
Dense	128	ReLU
Dense	128	ReLU
Output	10	Sigmoid

Table 3
Material properties used in this paper.

E_{11}/E_{22}	25
$E_{22}/E_{22} = E_{33}/E_{22}$	1
$G_{12}/E_{22} = G_{13}/E_{22}$	0.5
G_{23}/E_{22}	0.2
$\nu_{12} = \nu_{13} = \nu_{23}$	0.25

Table 4
$\bar{\omega}_1$, simply-supported shell with a/h = 10, [0°/90°/0°].

R/a	$\bar{\omega}_1$	$\bar{\omega}_1$ [30]
2	13.007	13.007
5	11.972	11.972
Plate	11.756	11.756

last convolutional layer is straightened into a one-dimensional array through the "Flatten" layer and passed to the second block of the network, made of two dense layers with 128 neurons, each adopting a ReLU as an activation function. Finally, the output of the CNN is obtained through the last layer with ten units, corresponding to the percentage errors over the first ten natural frequencies. For the training process, the network's hyperparameters update at each step was performed using the Adam optimizer [41], with a learning rate of 0.001. The loss function adopted was the Mean Absolute Percentage Error (MAPE), which provided the best results in the initial evaluation phase,

$$MAPE = \frac{1}{n}\sum_{i=1}^{n}\frac{|y^i - \hat{y}^i|}{y^i} \tag{31}$$

where n is the number of samples considered, y^i the ith expected value, and $\hat{y}^i$ the corresponding inferred one. A total of 500 training epochs and a batch size of 8 were used. The number of samples used to train the network was equal to the 10% of the 2^{12} considered theories. Depending on the number of active DOF, the number of theories with a given number of DOF changes. For each number of DOF, the number of randomly selected models was a percentage inversely proportional to its population. This selection process was designed to provide the network with a data set as informative as possible and achieve an improved generalization.

5. Numerical results

In this paper, various configurations of composite shells were analyzed by varying thickness, boundary conditions, and curvature radii, with the latter kept equal along α and β. The normalized material properties are summarized in Table 3. To lower the computational costs, a quarter of a square shell was considered and meshed with 4 × 4 Q9 elements. Symmetry boundary conditions were applied; therefore, only symmetrical modal shapes were considered. An ESL formulation was used, and the full fourth-order E4 Taylor expansion was assumed as the reference model.

First, a preliminary assessment was conducted to ensure the quality of the FE discretization. As a reference, the results on the first natural frequency provided in [30] were used, obtained using a full fourth-order Taylor expansion. Table 4 shows the results for a simply-supported shell, and a perfect match was found between the reference and the obtained values, reported in the non-dimensionalized form:

$$\bar{\omega} = \omega\sqrt{\frac{\rho a^4}{h^2 E_{22}}} \tag{32}$$

where ρ represents the density of the material, a is the side length of the structure, h is the thickness, and E_{22} the material's elastic modulus in direction "2". The same verification was performed for a clamped–free shell, see Table 5.

Table 5
$\bar{\omega}_1$, clamped–free shell with R/a = 10, [0°/90°/0°].

a/h	$\bar{\omega}_1$	$\bar{\omega}_1$ [30]
4	7.250	7.250
20	24.144	24.144

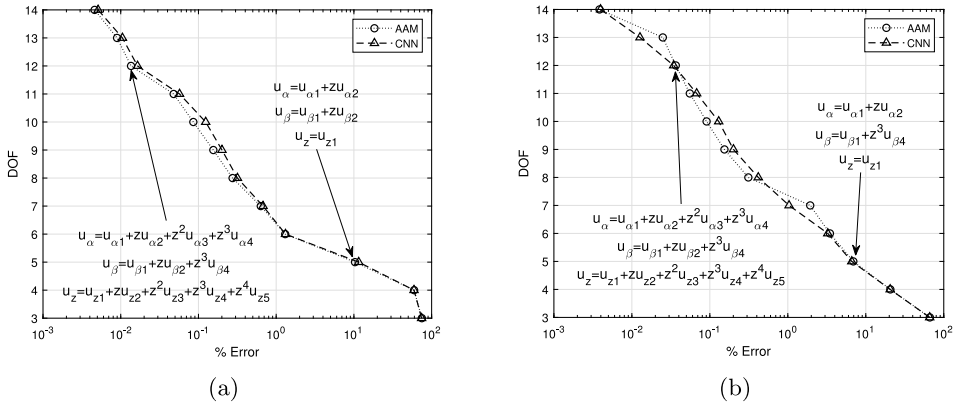

Fig. 5. BTD for simply-supported shell with R/a=2 - (a) I natural frequency, (b) II natural frequency.

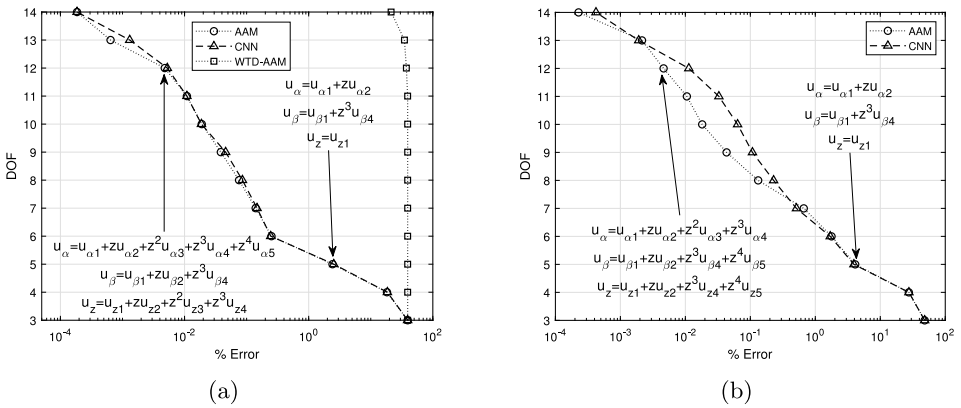

Fig. 6. BTD and WTD for simply-supported shell with R/a=2 - (a) III natural frequency, (b) IV natural frequency.

5.1. Simply-supported

The first numerical case considered a simply-supported shell with a/h=10 and stacking sequence [0°/90°/0°]. Different values of curvature radii were used, R/a=2, 5, and infinite. BTD were evaluated using the AAM procedure and the CNN for the first ten natural frequencies. Figs. 5 to 7 show the BTD for the first five frequencies of the R/a=2 shell. 'AAM' indicates the results obtained by computing the frequencies of all combinations of structural theories stemming from the fifteen terms of a fourth-order set. 'CNN' indicates the results obtained by the convolutional neural network trained with 10% of all combinations. In each plot, two best sets are shown, i.e., structural theories providing the best accuracy for a given number of nodal DOFs. Furthermore, to quantify the worst accuracy for a given DOF, the Worst Theory Diagram (WTD) is also shown in Fig. 6a. Tables 6 to 8 show the best models with five, eight, and twelve DOF, respectively. The aim is to show how the set of best generalized displacement variables depends on the mode considered. Figs. 8 to 10 show BTDs for the R/a=5 case. Tables 9 to 11 show the best theories; for the sake of brevity, five frequencies were reported instead of ten. To verify the accuracy of the best theories concerning the modal shapes, Fig. 11 shows the first five modes obtained with the 8-DOF best theories and compared with the ones stemming from the reference, full E4 model reported in Fig. 12. The results for the plate case are reported in Figs. 13 to 15 and Tables 12 to 14. The results obtained for the simply-supported case suggest the following:

- The CNN can reproduce the BTD for different frequencies with high accuracy using 10% of the computational overhead of the FEM approach. Furthermore, the best models built by considering natural frequencies as control parameters reproduce the modal shapes very well.

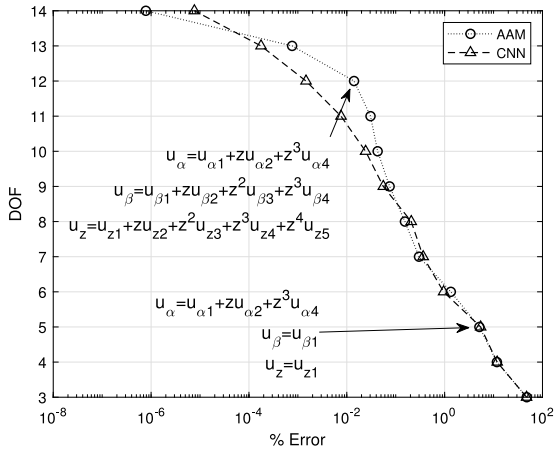

Fig. 7. BTD simply-supported shell with R/a=2 - V natural frequency.

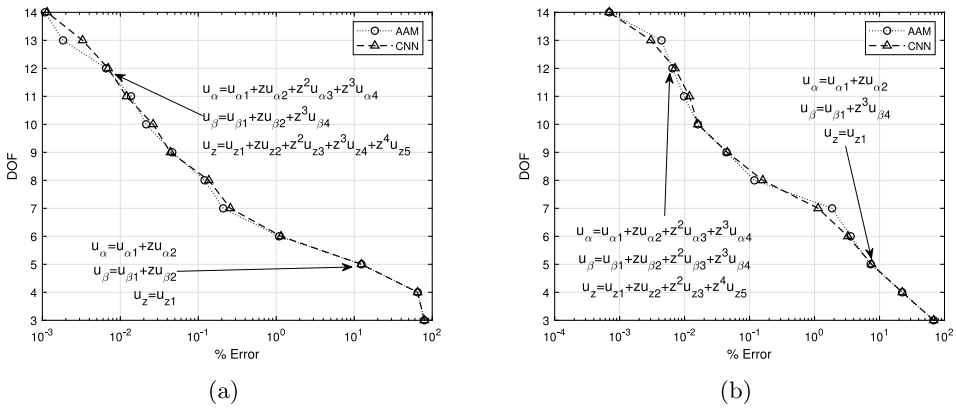

Fig. 8. BTD for simply-supported shell with R/a=5 - (a) I natural frequency, (b) II natural frequency.

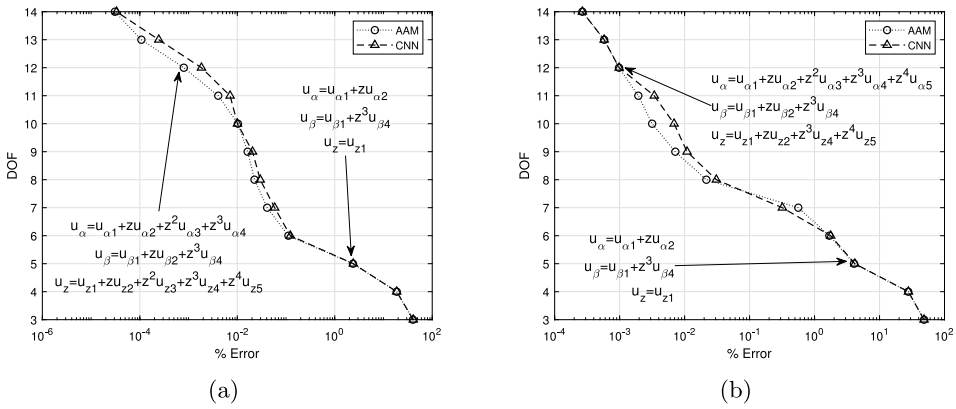

Fig. 9. BTD for simply-supported shell with R/a=5 - (a) III natural frequency, (b) IV natural frequency.

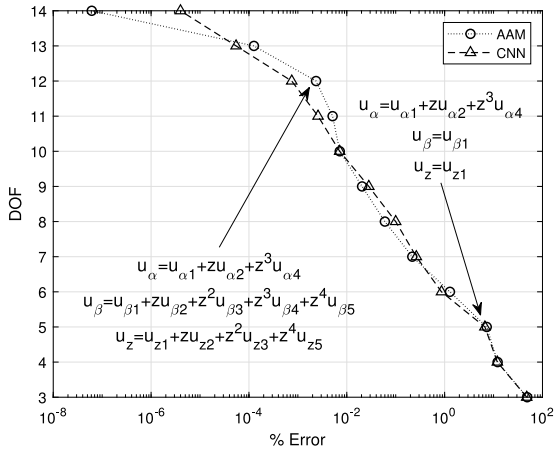

Fig. 10. BTD for simply-supported shell with R/a=5 - V natural frequency.

Table 6
Best theories with five DOF for the first ten frequencies, simply-supported shell with R/a = 2.

I					
u_α	▲	▲	△	△	△
u_β	▲	▲	△	△	△
u_z	▲	△	△	△	△

II					
u_α	▲	▲	△	△	△
u_β	▲	△	△	▲	△
u_z	▲	△	△	△	△

III					
u_α	▲	▲	△	△	△
u_β	▲	△	△	▲	△
u_z	▲	△	△	△	△

IV					
u_α	▲	▲	△	△	△
u_β	▲	△	△	▲	△
u_z	▲	△	△	△	△

V					
u_α	▲	▲	△	▲	△
u_β	▲	△	△	△	△
u_z	▲	△	△	△	△

VI					
u_α	▲	▲	△	△	△
u_β	▲	△	△	▲	△
u_z	▲	△	△	△	△

VII					
u_α	▲	▲	△	△	△
u_β	▲	△	△	▲	△
u_z	▲	△	△	△	△

VIII					
u_α	▲	▲	△	△	△
u_β	▲	△	△	▲	△
u_z	▲	△	△	△	△

IX					
u_α	▲	▲	△	△	△
u_β	▲	△	△	▲	△
u_z	▲	△	△	△	△

X					
u_α	▲	▲	△	▲	△
u_β	▲	△	△	△	△
u_z	▲	△	△	△	△

- Best theories depend on the mode number. As the number of waves increases, the role of higher-order generalized displacement variables becomes more critical, with third-order terms becoming necessary for the best accuracy.
- FSDT is a best theory for the first mode.
- Transverse stretching is often necessary to have errors smaller than 1%.
- The role of the curvature is not particularly relevant for choosing the best set of displacement variables.
- The WTD presented for the third natural frequency of the R/a=2 case shows the lower limit's behavior for the accuracy of a structural theory. Even higher-order models can suffer from significant errors.

5.2. Clamped–free

This section focuses on a different set of boundary conditions and the effect of thickness. The shell has two opposite edges clamped and the other two free; R/a=10. Figs. 16 to 18 show BTDs for a/h=20, whereas Tables 15 to 17 presents the best theories for the first five frequencies. The results for the thick case with a/h=4, are shown in Figs. 19 to 21 and Tables 18 to 20. The numerical results suggest that

Table 7
Best theories with eight DOF for the first ten frequencies, simply-supported shell with R/a = 2.

I					
u_α	▲	▲	△	△	△
u_β	▲	▲	△	▲	△
u_z	▲	▲	▲	△	△

II					
u_α	▲	▲	△	▲	△
u_β	▲	▲	△	▲	△
u_z	▲	△	▲	△	△

III					
u_α	▲	▲	△	△	△
u_β	▲	▲	△	▲	△
u_z	▲	▲	▲	△	△

IV					
u_α	▲	▲	△	▲	△
u_β	▲	▲	△	▲	△
u_z	▲	△	△	△	▲

V					
u_α	▲	▲	△	▲	△
u_β	▲	▲	△	▲	△
u_z	▲	△	△	△	▲

VI					
u_α	▲	▲	△	▲	△
u_β	▲	▲	△	▲	△
u_z	▲	△	△	△	▲

VII					
u_α	▲	▲	△	△	△
u_β	▲	▲	△	▲	△
u_z	▲	▲	▲	△	△

VIII					
u_α	▲	△	▲	▲	▲
u_β	▲	△	△	▲	△
u_z	▲	▲	△	△	△

IX					
u_α	▲	▲	▲	△	▲
u_β	▲	▲	△	▲	△
u_z	▲	△	△	△	△

X					
u_α	▲	▲	△	▲	△
u_β	▲	△	△	▲	△
u_z	▲	△	▲	△	▲

Table 8
Best theories with twelve DOF for the first ten frequencies, simply-supported shell with R/a = 2.

I					
u_α	▲	▲	▲	▲	△
u_β	▲	▲	△	▲	△
u_z	▲	▲	▲	▲	▲

II					
u_α	▲	▲	▲	▲	△
u_β	▲	▲	△	▲	△
u_z	▲	▲	▲	▲	▲

III					
u_α	▲	▲	▲	▲	▲
u_β	▲	▲	△	▲	△
u_z	▲	▲	▲	▲	△

IV					
u_α	▲	▲	▲	▲	△
u_β	▲	▲	△	▲	▲
u_z	▲	▲	△	▲	▲

V					
u_α	▲	▲	△	▲	△
u_β	▲	▲	▲	▲	△
u_z	▲	▲	▲	▲	▲

VI					
u_α	▲	▲	▲	▲	△
u_β	▲	▲	△	▲	△
u_z	▲	▲	▲	▲	▲

VII					
u_α	▲	▲	▲	▲	▲
u_β	▲	▲	△	▲	△
u_z	▲	▲	▲	▲	△

VIII					
u_α	▲	▲	▲	△	▲
u_β	▲	△	▲	▲	▲
u_z	▲	▲	▲	△	▲

IX					
u_α	▲	▲	▲	▲	▲
u_β	▲	▲	▲	▲	△
u_z	▲	▲	▲	△	△

X					
u_α	▲	▲	△	▲	△
u_β	▲	▲	▲	▲	△
u_z	▲	▲	▲	▲	▲

Table 9
Best theories with five DOF for the first five frequencies, simply-supported shell with R/a = 5.

I					
u_α	▲	▲	△	△	△
u_β	▲	▲	△	△	△
u_z	▲	△	△	△	△

II					
u_α	▲	▲	△	△	△
u_β	▲	△	△	▲	△
u_z	▲	△	△	△	△

III					
u_α	▲	▲	△	△	△
u_β	▲	△	△	▲	△
u_z	▲	△	△	△	△

IV					
u_α	▲	▲	△	△	△
u_β	▲	△	△	▲	△
u_z	▲	△	△	△	△

V					
u_α	▲	▲	△	▲	△
u_β	▲	△	△	△	△
u_z	▲	△	△	△	△

Table 10
Best theories with eight DOF for the first five frequencies, simply-supported shell with R/a = 5.

I					
u_α	▲	▲	△	▲	△
u_β	▲	▲	△	▲	△
u_z	▲	△	▲	△	△

II					
u_α	▲	▲	△	▲	△
u_β	▲	▲	△	▲	△
u_z	▲	△	△	△	▲

III					
u_α	▲	▲	△	△	△
u_β	▲	▲	△	▲	△
u_z	▲	▲	△	△	▲

IV					
u_α	▲	▲	△	▲	△
u_β	▲	▲	△	▲	△
u_z	▲	△	△	△	▲

V					
u_α	▲	▲	△	▲	△
u_β	▲	▲	△	▲	△
u_z	▲	△	△	△	▲

Table 11
Best theories with twelve DOF for the first five frequencies, simply-supported shell with R/a = 5.

I					
u_α	▲	▲	▲	▲	△
u_β	▲	▲	△	▲	△
u_z	▲	▲	▲	▲	▲

II					
u_α	▲	▲	▲	▲	△
u_β	▲	▲	▲	▲	△
u_z	▲	▲	▲	△	▲

III					
u_α	▲	▲	▲	▲	△
u_β	▲	▲	△	▲	△
u_z	▲	▲	▲	▲	▲

IV					
u_α	▲	▲	▲	▲	▲
u_β	▲	▲	△	▲	△
u_z	▲	▲	△	▲	▲

V					
u_α	▲	▲	△	▲	△
u_β	▲	▲	▲	▲	▲
u_z	▲	▲	▲	△	▲

Table 12
Best theories with five DOF for the first five frequencies, simply-supported plate.

I					
u_α	▲	▲	△	△	△
u_β	▲	▲	△	△	△
u_z	▲	△	△	△	△

II					
u_α	▲	▲	△	△	△
u_β	▲	△	△	▲	△
u_z	▲	△	△	△	△

III					
u_α	▲	▲	△	△	△
u_β	▲	△	△	▲	△
u_z	▲	△	△	△	△

IV					
u_α	▲	▲	△	△	△
u_β	▲	△	△	▲	△
u_z	▲	△	△	△	△

V					
u_α	▲	▲	△	▲	△
u_β	▲	△	△	△	△
u_z	▲	△	△	△	△

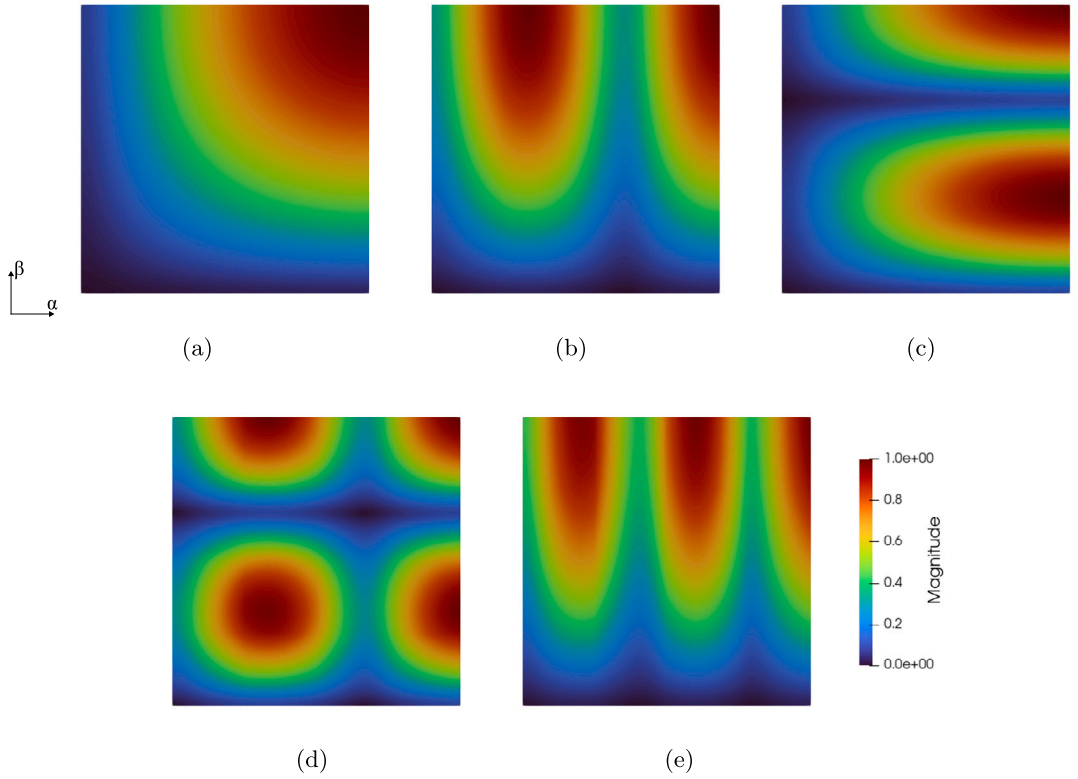

Fig. 11. First five modes obtained using the best 8-DOF theories, simply-supported shell with R/a=5 - (a) Mode I, (b) Mode II, (c) Mode III, (d) Mode IV, (e) Mode V.

Table 13
Best theories with eight DOF for the first five frequencies, simply-supported plate.

I					
u_α	▲	▲	△	△	△
u_β	▲	▲	△	▲	△
u_z	▲	▲	▲	△	△

II					
u_α	▲	▲	△	▲	△
u_β	▲	▲	△	▲	△
u_z	▲	△	△	△	▲

III					
u_α	▲	▲	△	△	△
u_β	▲	▲	△	▲	△
u_z	▲	▲	△	△	▲

IV					
u_α	▲	▲	△	▲	△
u_β	▲	▲	△	▲	△
u_z	▲	△	△	△	▲

V					
u_α	▲	▲	△	▲	△
u_β	▲	▲	△	▲	△
u_z	▲	△	△	△	▲

Table 14
Best theories with twelve DOF for the first five frequencies, simply-supported plate.

I					
u_α	▲	▲	▲	▲	△
u_β	▲	▲	▲	▲	△
u_z	▲	▲	▲	▲	△

II					
u_α	▲	▲	▲	▲	△
u_β	▲	▲	△	▲	△
u_z	▲	▲	▲	▲	▲

III					
u_α	▲	▲	▲	▲	▲
u_β	▲	▲	△	▲	▲
u_z	▲	▲	△	△	▲

IV					
u_α	▲	▲	▲	▲	△
u_β	▲	▲	▲	▲	△
u_z	▲	▲	△	▲	▲

V					
u_α	▲	▲	△	▲	△
u_β	▲	▲	▲	▲	△
u_z	▲	▲	▲	▲	▲

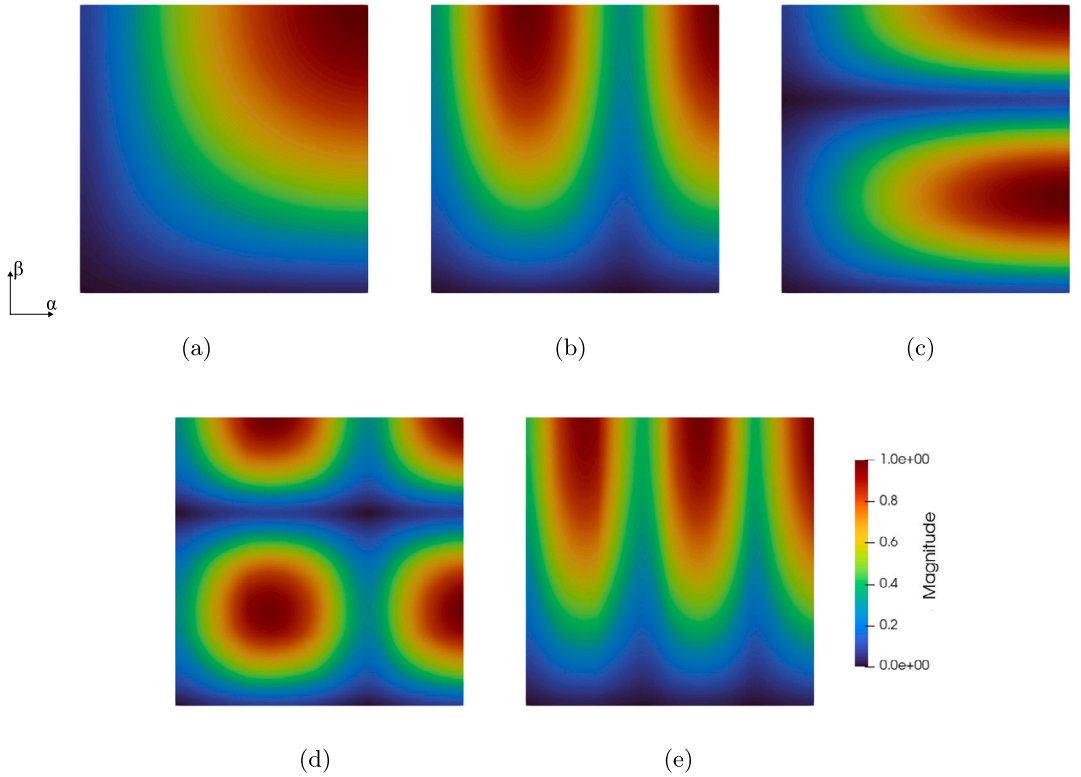

Fig. 12. First five modes obtained using the full E4 theory, simply-supported shell with R/a=5 - (a) Mode I, (b) Mode II, (c) Mode III, (d) Mode IV, (e) Mode V.

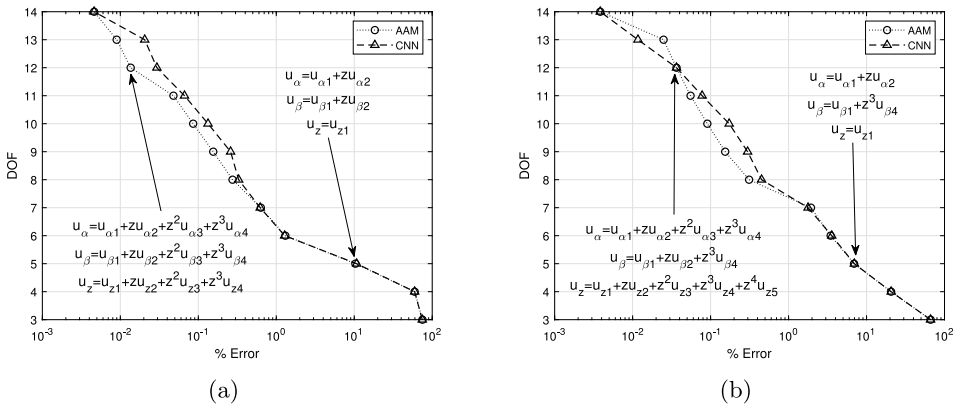

Fig. 13. BTD for simply-supported plate - (a) I natural frequency, (b) II natural frequency.

- The thickness of the shell has a predominant role in the definition of the best theories. The thickness is the most relevant among the parameters considered in this paper.
- As the shell becomes thick, the higher-order terms are mandatory to obtain acceptable accuracy. Five Best models with five DOFs are no more FSDT as third-order terms are necessary.
- The role of transverse stretching remains crucial for accuracy.

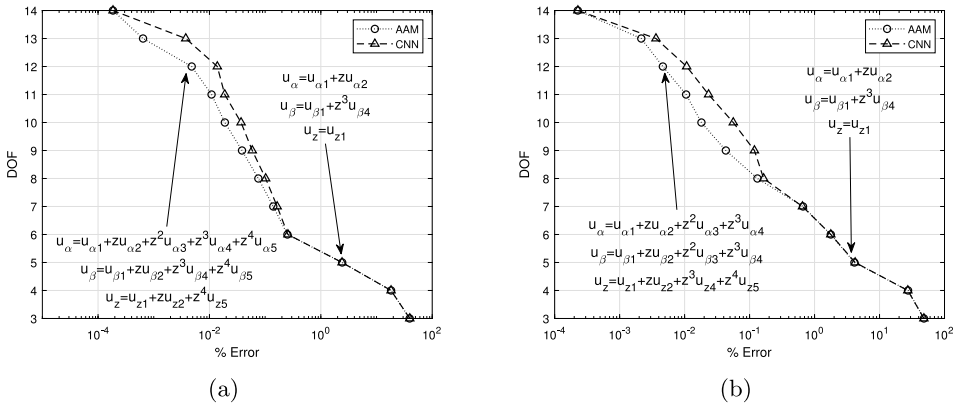

Fig. 14. BTD for simply-supported plate - (a) III natural frequency, (b) IV natural frequency.

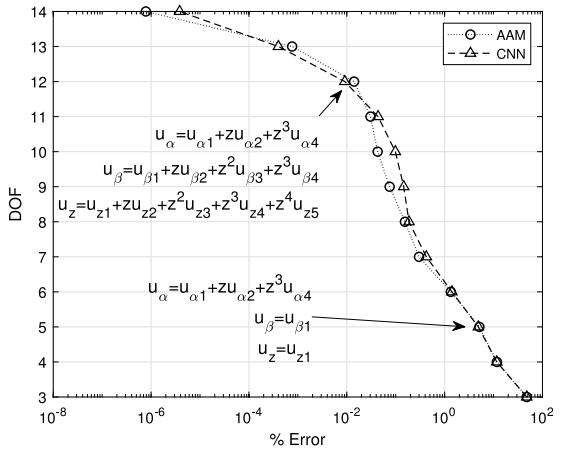

Fig. 15. BTD for simply-supported plate - V natural frequency.

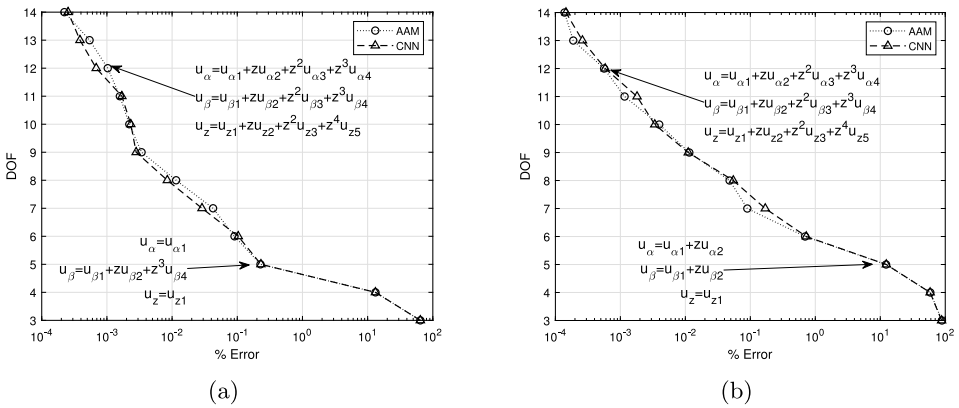

Fig. 16. BTD for clamped–free shell with a/h=20 - (a) I natural frequency, (b) II natural frequency.

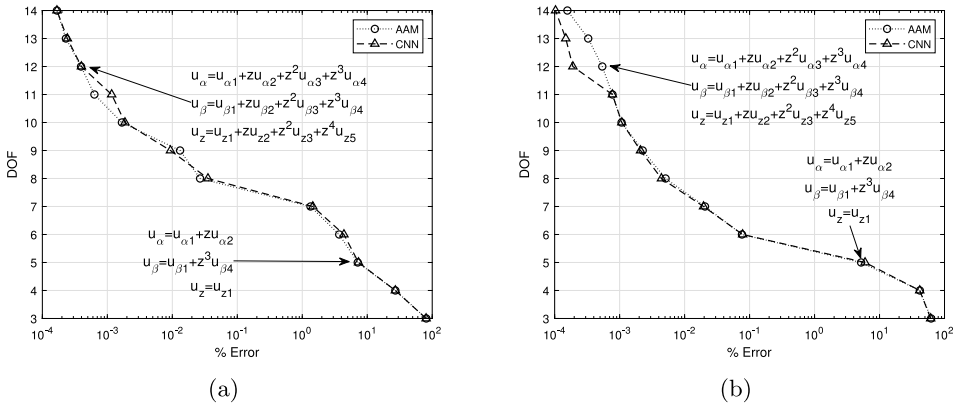

Fig. 17. BTD for clamped–free shell with a/h=20 - (a) III natural frequency, (b) IV natural frequency.

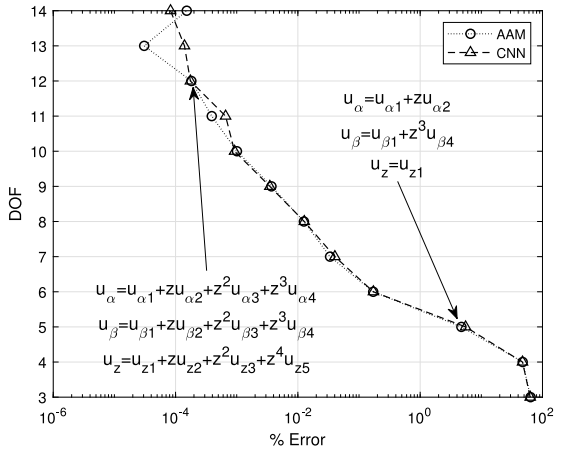

Fig. 18. BTD for clamped–free shell with a/h=20 - V natural frequency.

Table 15
Best theories with five DOF, clamped–free shell with a/h = 20.

I					
u_α	▲	△	△	△	△
u_β	▲	▲	△	▲	△
u_z	▲	△	△	△	△

II					
u_α	▲	▲	△	△	△
u_β	▲	▲	△	△	△
u_z	▲	△	△	△	△

III					
u_α	▲	▲	△	△	△
u_β	▲	△	△	▲	△
u_z	▲	△	△	△	△

IV					
u_α	▲	▲	△	△	△
u_β	▲	△	△	▲	△
u_z	▲	△	△	△	△

V					
u_α	▲	▲	△	△	△
u_β	▲	△	△	▲	△
u_z	▲	△	△	△	△

Table 16
Best theories with eight DOF, clamped–free shell with a/h = 20.

I					
u_α	▲	▲	△	△	△
u_β	▲	▲	△	▲	△
u_z	▲	▲	▲	△	△

II					
u_α	▲	▲	△	▲	△
u_β	▲	▲	△	▲	△
u_z	▲	△	▲	△	△

III					
u_α	▲	▲	△	▲	△
u_β	▲	▲	△	▲	△
u_z	▲	△	▲	△	△

IV					
u_α	▲	▲	△	△	△
u_β	▲	▲	△	▲	△
u_z	▲	△	▲	△	▲

V					
u_α	▲	▲	△	△	△
u_β	▲	▲	△	▲	△
u_z	▲	△	▲	△	▲

Table 17
Best theories with twelve DOF, clamped–free shell with a/h = 20.

I					
u_α	▲	▲	▲	▲	△
u_β	▲	▲	▲	▲	△
u_z	▲	▲	▲	△	▲

II					
u_α	▲	▲	▲	▲	△
u_β	▲	▲	▲	▲	△
u_z	▲	▲	▲	△	▲

III					
u_α	▲	▲	▲	▲	△
u_β	▲	▲	▲	▲	△
u_z	▲	▲	▲	△	▲

IV					
u_α	▲	▲	▲	▲	△
u_β	▲	▲	▲	▲	△
u_z	▲	▲	▲	△	▲

V					
u_α	▲	▲	▲	▲	△
u_β	▲	▲	▲	▲	△
u_z	▲	▲	▲	△	▲

Table 18
Best theories with five DOF, clamped–free shell with a/h = 4.

I					
u_α	▲	△	△	△	△
u_β	▲	▲	△	▲	△
u_z	▲	△	△	△	△

II					
u_α	▲	▲	△	△	△
u_β	▲	△	△	▲	△
u_z	▲	△	△	△	△

III					
u_α	▲	△	△	△	△
u_β	▲	▲	△	▲	△
u_z	▲	△	△	△	△

IV					
u_α	▲	▲	△	△	△
u_β	▲	△	△	▲	△
u_z	▲	△	△	△	△

V					
u_α	▲	▲	△	△	△
u_β	▲	△	△	▲	△
u_z	▲	△	△	△	△

Table 19
Best theories with eight DOF, clamped–free shell with a/h = 4.

I					
u_α	▲	△	△	▲	△
u_β	▲	▲	△	▲	△
u_z	▲	△	▲	△	▲

II					
u_α	▲	▲	△	▲	△
u_β	▲	▲	△	▲	△
u_z	▲	△	▲	△	△

III					
u_α	▲	▲	△	▲	△
u_β	▲	▲	△	▲	△
u_z	▲	△	▲	△	△

IV					
u_α	▲	▲	△	▲	△
u_β	▲	▲	△	▲	△
u_z	▲	△	▲	△	△

V					
u_α	▲	▲	△	▲	△
u_β	▲	▲	△	▲	△
u_z	▲	△	▲	△	△

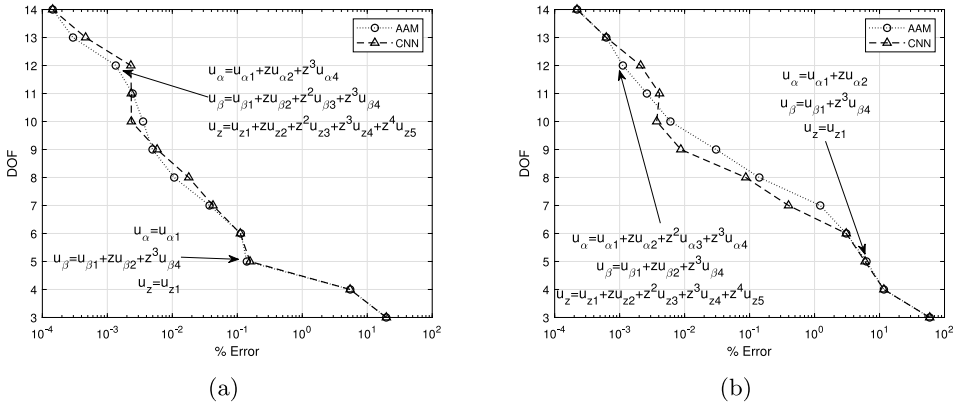

Fig. 19. BTD for clamped–free shell with a/h=4 - (a) I natural frequency, (b) II natural frequency.

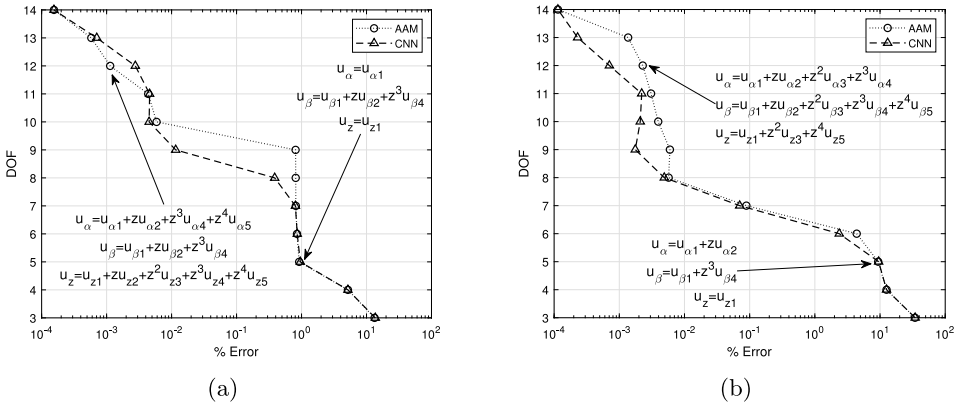

Fig. 20. BTD for clamped–free shell with a/h=4 - (a) III natural frequency, (b) IV natural frequency.

Table 20
Best theories with twelve DOF, clamped–free shell with a/h = 4.

I					
u_α	▲	▲	△	▲	△
u_β	▲	▲	▲	▲	△
u_z	▲	▲	▲	▲	▲

II					
u_α	▲	▲	▲	▲	△
u_β	▲	▲	△	▲	△
u_z	▲	▲	▲	▲	▲

III					
u_α	▲	▲	△	▲	▲
u_β	▲	▲	△	▲	△
u_z	▲	▲	▲	▲	▲

IV					
u_α	▲	▲	▲	▲	△
u_β	▲	▲	▲	▲	▲
u_z	▲	△	▲	△	▲

V					
u_α	▲	▲	▲	▲	▲
u_β	▲	▲	△	▲	△
u_z	▲	▲	▲	△	▲

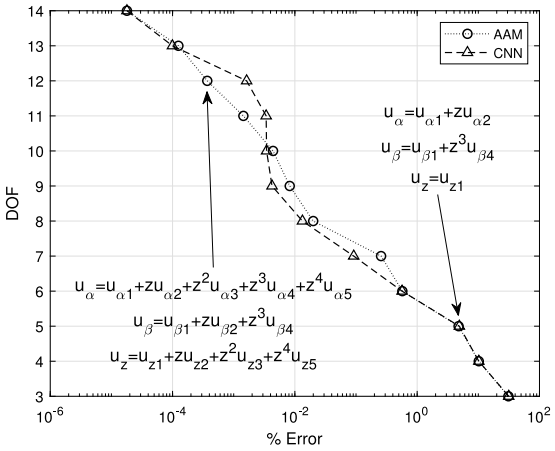

Fig. 21. BTD for clamped–free shell with a/h=4 - V natural frequency.

6. Conclusions

This paper investigated the adoption of a Convolutional Neural Network to find the best structural theories for the free vibration analysis of composite shells. The focus was on Equivalent Single Layer models with higher-order expansions up to the fourth-order. CNN was trained using finite element analyses carried out using the Carrera Unified Formulation. CNN training features included the active generalized displacement variables, i.e., the structural theory, and the first ten frequencies were the output. Best Theory Diagrams were built using the Axiomatic/Asymptotic Method for different shell configurations, providing us with the reference results for the evaluation of the performance and reliability of the network. In doing so, the role of structural parameters such as thickness, curvature, and boundary conditions on the accuracy of a specific model was also investigated. From the analysis of the best theories and BTDs obtained using the newly developed ML approach, it can be observed that:

- The CNN can successfully identify the best theories for a specific structural configuration. The accuracy was verified using reference finite element results, and excellent matches were found. A CNN can thus be used to test the accuracy of any structural theory for a given set of parameters, providing essential guidelines on the modeling strategy.
- The training of the CNN required only a limited pool of data, equal to 10% of the total amount of possible combinations of expansion terms, leading to a drastic reduction of computational overhead compared to previous works based solely on finite element computations. The computation of the BTD through CNN required, on average, 10% of the computational time of the complete FE analysis. The training process requires a fraction of the time needed for an FE analysis, and the total cost is related to the size of the training set.
- Another advantage the CNN brings is the possibility of operating with multiple outputs, thus being capable, if appropriately trained, of providing information regarding different indicators simultaneously, possibly leading to the definition of an overall performance score.
- The analysis of the best theories highlighted the critical role of third-order terms as the number of waves increases. Furthermore, the thickness of the shell is the predominant factor for the choice of the structural theory. For thick shells, third-order terms and transverse stretching are mandatory for acceptable accuracy.
- The discrepancies observed between the results generated by the AAM and the CNN are primarily located in the top part of the BTD, where errors are low, and the number of combinations is low. For instance, there are only fourteen theories with fourteen DOF, and the training process may be affected by such a low number of samples.
- The newly developed ML approach can be extended to virtually any structure to help define the optimal modeling approach. Different categories of structural models can also be considered, e.g., those using different mathematical formulations for the expansion functions or having different geometries, e.g., spherical shells and beams.

Future works will extend the present approach to time domain responses. There may be different strategies: machine learning could be trained to provide the modes to be used for superposition or could directly provide the time response.

CRediT authorship contribution statement

M. Petrolo: Conceptualization, Data curation, Investigation, Methodology, Writing – original draft, Writing – review & editing. **P. Iannotti:** Conceptualization, Data curation, Investigation, Methodology, Writing – original draft, Writing – review & editing.

M. Trombini: Conceptualization, Data curation, Investigation, Methodology, Writing – original draft, Writing – review & editing. **A. Pagani:** Conceptualization, Data curation, Investigation, Methodology, Writing – original draft, Writing – review & editing. **E. Carrera:** Conceptualization, Data curation, Investigation, Methodology, Writing – original draft, Writing – review & editing.

Declaration of competing interest

The authors declare that they have no known competing financial interests or personal relationships that could have appeared to influence the work reported in this paper.

Data availability

Data will be made available on request.

Acknowledgment

This research has received no external funding.

References

[1] F.B Hildebrand, E. Reissner, G.B. Thomas, Notes on the Foundations of the Theory of Small Displacements of Orthotropic Shells, Tech. Rep., Massachusetts Institute of Technology, 1949, URL: https://ntrs.nasa.gov/citations/19930082518.
[2] B.F. Vlasov, On the equations of bending of plates, Dokla Ak Nauk Azerbeijanskoi-SSR 3 (1957) 955–979.
[3] J.N. Reddy, A simple higher-order theory for laminated composite plates, J. Appl. Mech. 51 (4) (1984) 745–752, http://dx.doi.org/10.1115/1.3167719, arXiv:https://asmedigitalcollection.asme.org/appliedmechanics/article-pdf/51/4/745/5457622/745_1.pdf.
[4] J.N. Reddy, N.D. Phan, Stability and vibration of isotropic, orthotropic and laminated plates according to a higher-order shear deformation theory, J. Sound Vib. 98 (2) (1985) 157–170, http://dx.doi.org/10.1016/0022-460X(85)90383-9.
[5] C. Ossadzow, M. Touratier, An improved shear-membrane theory for multilayered shells, Compos. Struct. 52 (1) (2001) 85–95, http://dx.doi.org/10.1016/S0263-8223(00)00194-X.
[6] A.J.M. Ferreira, E. Carrera, M. Cinefra, C.M.C. Roque, O. Polit, Analysis of laminated shells by a sinusoidal shear deformation theory and radial basis functions collocation, accounting for through-the-thickness deformations, Compos. Part B-Eng. 42 (5) (2011) 1276–1284, http://dx.doi.org/10.1016/j.compositesb.2011.01.031.
[7] J.L. Mantari, A.S. Oktem, C. Guedes Soares, Bending and free vibration analysis of isotropic and multilayered plates and shells by using a new accurate higher-order shear deformation theory, Compos. Part B-Eng. 43 (8) (2012) 3348–3360, http://dx.doi.org/10.1016/j.compositesb.2012.01.062.
[8] A.S. Sayyad, Y.M. Ghugal, Static and free vibration analysis of laminated composite and sandwich spherical shells using a generalized higher-order shell theory, Compos. Struct. 219 (2019) 129–146, http://dx.doi.org/10.1016/j.compstruct.2019.03.054.
[9] D.S. Mashat, E. Carrera, A.M. Zenkour, S.A. Al Khateeb, Axiomatic/asymptotic evaluation of multilayered plate theories by using single and multi-points error criteria, Compos. Struct. 106 (2013) 393–406, http://dx.doi.org/10.1016/j.compstruct.2013.05.047.
[10] M. Petrolo, M. Cinefra, A. Lamberti, E. Carrera, Evaluation of mixed theories for laminated plates through the axiomatic/asymptotic method, Compos. Part B-Eng. 76 (2015) 260–272, http://dx.doi.org/10.1016/j.compositesb.2015.02.027.
[11] S. Candiotti, J.L. Mantari, J. Yarasca, M. Petrolo, E. Carrera, An axiomatic/asymptotic evaluation of best theories for isotropic metallic and functionally graded plates employing non-polynomic functions, Aerosp. Sci. Technol. 68 (2017) 179–192, http://dx.doi.org/10.1016/j.ast.2017.05.003.
[12] E. Carrera, M. Petrolo, Guidelines and recommendations to construct theories for metallic and composite plates, AIAA J. 48 (12) (2010) 2852–2866, http://dx.doi.org/10.2514/1.J050316.
[13] E. Carrera, M. Petrolo, On the effectiveness of higher-order terms in refined beam theories, J. Appl. Mech. 78 (2) (2011) 021013, http://dx.doi.org/10.1115/1.4002207.
[14] E. Carrera, M. Cinefra, A. Lamberti, M. Petrolo, Results on best theories for metallic and laminated shells including layer-wise models, Compos. Struct. 126 (2015) 285–298, http://dx.doi.org/10.1016/j.compstruct.2015.02.027.
[15] B. Cheng, D.M. Titterington, Neural Networks: A review from a statistical perspective, Stat. Sci. 9 (1) (1994) 2–30, http://dx.doi.org/10.1214/ss/1177010638.
[16] M. Zakaria, M. Al-Shebany, S. Sarhan, Artificial neural network: a brief overview, Int. J. Eng. Res. Appl. 4 (2) (2014) 7–12, URL: https://www.ijera.com/papers/Vol4_issue2/Version%201/B42010712.pdf.
[17] H.T. Thai, Machine learning for structural engineering: A state-of-the-art review, Struct. 38 (2022) 448–491, http://dx.doi.org/10.1016/j.istruc.2022.02.003.
[18] G. Balokas, S. Czichon, R. Rolfes, Neural network assisted multiscale analysis for the elastic properties prediction of 3D braided composites under uncertainty, Compos. Struct. 183 (2018) 550–562, http://dx.doi.org/10.1016/j.compstruct.2017.06.037.
[19] P. Gustafson, E. Pineda, T. Ricks, B. Bednarcyk, B. Hearley, J. Stuckner, Convolutional neural network for enhancement of localization in granular representative unit cells, AIAA J. 61 (2023) 1–13, http://dx.doi.org/10.2514/1.J061918.
[20] M.G. Vineela, A. Dave, P.K. Chaganti, Artificial neural network based prediction of tensile strength of hybrid composites, Mater. Today-Proc. 5 (9, Part 3) (2018) 19908–19915, http://dx.doi.org/10.1016/j.matpr.2018.06.356, Materials Processing and characterization, 16th – 18th March 2018.
[21] A. Pagani, M. Enea, E. Carrera, Component-wise damage detection by neural networks and refined FEs training, J. Sound Vib. 509 (2021) 116255, http://dx.doi.org/10.1016/j.jsv.2021.116255.
[22] J. Gajewski, P. Golewski, T. Sadowski, Geometry optimization of a thin-walled element for an air structure using hybrid system integrating artificial neural network and finite element method, Compos. Struct. 159 (2017) 589–599, http://dx.doi.org/10.1016/j.compstruct.2016.10.007.
[23] F. Tao, X. Liu, H. Du, S. Tian, W. Yu, Discover failure criteria of composites from experimental data by sparse regression, Compos. Part B-Eng. 239 (2022) 109947, http://dx.doi.org/10.1016/j.compositesb.2022.109947.
[24] C.A. Yan, R. Vescovini, L. Dozio, A framework based on physics-informed neural networks and extreme learning for the analysis of composite structures, Comput. Struct. 265 (2022) 106761, http://dx.doi.org/10.1016/j.compstruc.2022.106761.
[25] K.D. Humfeld, D. Gu, G.A. Butler, K. Nelson, N. Zobeiry, A machine learning framework for real-time inverse modeling and multi-objective process optimization of composites for active manufacturing control, Compos. Part B-Eng. 223 (2021) 109150, http://dx.doi.org/10.1016/j.compositesb.2021.109150.
[26] K. O'Shea, R. Nash, An introduction to convolutional neural networks, 2015, http://dx.doi.org/10.48550/arXiv.1511.08458, CoRR. arXiv:1511.08458.

[27] S. Albawi, T.A. Mohammed, S. Al-Zawi, Understanding of a convolutional neural network, in: 2017 International Conference on Engineering and Technology, ICET, 2017, pp. 1–6, http://dx.doi.org/10.1109/ICEngTechnol.2017.8308186.
[28] J. Gu, Z. Wang, J. Kuen, L. Ma, A. Shahroudy, B. Shuai, T. Liu, X. Wang, G. Wang, J. Cai, T. Chen, Recent advances in convolutional neural networks, Pattern Recognit. 77 (2018) 354–377, http://dx.doi.org/10.1016/j.patcog.2017.10.013.
[29] M. Petrolo, E. Carrera, On the use of neural networks to evaluate performances of shell models for composites, Adv. Model. Simul. Eng. Sci. 7 (31) (2020) http://dx.doi.org/10.1186/s40323-020-00169-y.
[30] M. Petrolo, E. Carrera, Methods and guidelines for the choice of shell theories, Acta Mech. 231 (2020) 395–434, http://dx.doi.org/10.1007/s00707-019-02601-w.
[31] M. Petrolo, E. Carrera, Selection of element-wise shell kinematics using neural networks, Comput. Struct. 244 (2021) 106425, http://dx.doi.org/10.1016/j.compstruc.2020.106425.
[32] E. Carrera, Theories and finite elements for multilayered plates and shells: A unified compact formulation with numerical assessment and benchmarking, Arch. Comput. Method. E. 10 (2003) 215–296, http://dx.doi.org/10.1007/BF02736224.
[33] N.N. Rogacheva, The Theory of Piezoelectric Shells and Plates, CRC Press, Boca Raton, 2020, http://dx.doi.org/10.1201/9781003068129.
[34] E. Carrera, M. Cinefra, M. Petrolo, E. Zappino, Finite Element Analysis of Structures Through Unified Formulation, Wiley, Chichester, 2014, http://dx.doi.org/10.1002/9781118536643.
[35] K.J. Bathe, E.N. Dvorkin, A formulation of general shell elements — the use of mixed interpolation of tensorial components, Internat. J. Numer. Methods Engrg. 22 (3) (1986) 697–722, http://dx.doi.org/10.1002/nme.1620220312.
[36] M.L. Bucalem, K.-J. Bathe, Higher-order MITC general shell elements, Internat. J. Numer. Methods Engrg. 36 (21) (1993) 3729–3754, http://dx.doi.org/10.1002/nme.1620362109.
[37] J.N. Reddy, Mechanics of Laminated Composite Plates - Theory and Analysis, CRC Press, Boca Raton, 1997, http://dx.doi.org/10.1201/b12409.
[38] S.W. Tsai, Composites Design, Vol. 5, Think composites, Dayton, 1988.
[39] M. Cinefra, S. Valvano, A variable kinematic doubly-curved MITC9 shell element for the analysis of laminated composites, Mech. Adv. Mater. Struct. 23 (2015) 1312–1325, http://dx.doi.org/10.1080/15376494.2015.1070304.
[40] M. Petrolo, E. Carrera, Best spatial distributions of shell kinematics over 2D meshes for free vibration analyses, Aerotec. Missili Spaz. 99 (2020) 217–232, http://dx.doi.org/10.1007/s42496-020-00045-3.
[41] D.P. Kingma, J. Ba, Adam: A method for stochastic optimization, 2015, http://dx.doi.org/10.48550/arXiv.1412.6980, arXiv:1412.6980.